Featured in Physics

Shooting Rubber Bands: Two Self-Similar Retractions for a Stretched Elastic Wedge

Alexandros T. Oratis and James C. Bird[*]
Department of Mechanical Engineering, Boston University, Boston, Massachusetts 02215, USA

(Received 11 August 2018; published 4 January 2019)

Stretching and shooting rubber bands is a familiar experience for both children and adults, yet the initial dynamics are so quick that they are generally missed. When a cut elastic strip is stretched from its end and suddenly released, the dynamics depend on a balance of stretching and inertia. However, when a rubber band is stretched, a region of high curvature is created and it is unclear how this curvature affects the dynamics. Here, we demonstrate that during the retraction of a circular rubber band, a wavelength develops at the rear which increases in size as time progresses. Through a combination of experiments and modeling, we investigate the speed at which the back of the elastic retracts and observe a self-similar shape that depends on stretching, inertia, and bending. These retraction dynamics illuminate how a rubber band can pass by a thumb when discharged without hitting it.

DOI: 10.1103/PhysRevLett.122.014102

Stretching and shooting a rubber band is a familiar experience, enjoyed by children and adults alike. Yet, the process occurs so fast that the deformation goes unnoticed. Pinching and releasing a rubber band is closely related to the motion of a plucked string, a problem that has a rich history dating back to debates between Euler and D'Alembert [1]. Indeed, these types of retraction processes are ubiquitous and can be found across a variety of length scales, including on the strings of certain musical instruments [2], the release of an archer's bow [3], a 100-m slingshot ride at an amusement park, and the molecular slingshot motion of proposed drug-delivery nanomachines [4]. Although models of stretched elastic recoil are typically limited to the coupling of inertia and stretching [5–9], bending moments are known to be important in regions of high curvature [10–12]. In this Letter, we show that the shape of the retracting wedge depends on how much it is stretched, its wedge angle, and a time-varying dimensionless group that arises naturally from a balance of stretching and bending. For the shooting of a typical rubber band, we find that bending is important over the entire retraction period, manifested in a distinct self-similar dynamics that captures elements of stretching, bending, and inertia.

The motion of a circular rubber band as it is stretched and released is illustrated in Fig. 1. As the rubber band is stretched with strain ϵ, it straightens and forms a wedge with a half-angle ϕ and side length $(\epsilon + 1)\ell_0$. Upon release at time $t = 0$, the rubber band recoils with a speed V and develops a clear rounded region in the rear with a growing wavelength λ. Yet, the front of the elastic begins to move well before the rear reaches it, allowing the thumb to tuck out of the path of the rear of the elastic in time for it to pass [see the Supplemental Video [13]]. It is interesting to note that as the front begins to move, it dynamically buckles in a manner similar to that observed in straight beams and rods [14,15], although in this case it is not impacting a rigid object, and thus shares similarities with the front motion of a falling slinky [16]. These observations indicate the presence and importance of a longitudinal stress wave, which has been noted in the recoil of flat rubber strips [15,17].

To visualize and quantify this process more precisely, we carry out experiments in which the rubber band is looped around a cylinder and marked to track the motion of material points [Fig. 2(a)]. The motion of the marks allows us to identify the presence and location of the longitudinal

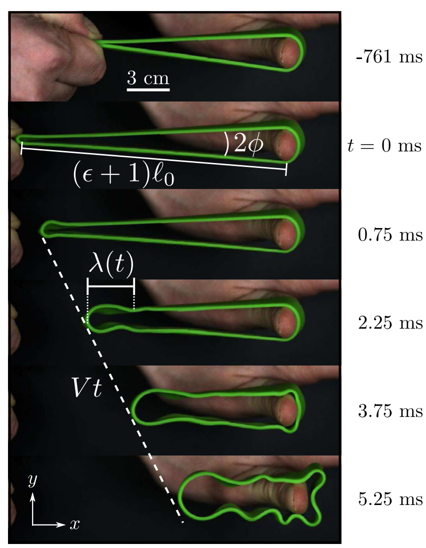

FIG. 1. High-speed images of a rubber band being pinched, stretched, and released, resulting in it being fired at approximately $V = 12.5$ m/s. Here the elastic is pulled back to form a wedge with a half-angle ϕ and length $(1 + \epsilon)\ell_0$, where ϵ is the strain. A key feature in the shape of the retracting elastic is a rounded region with a growing wavelength $\lambda(t)$.

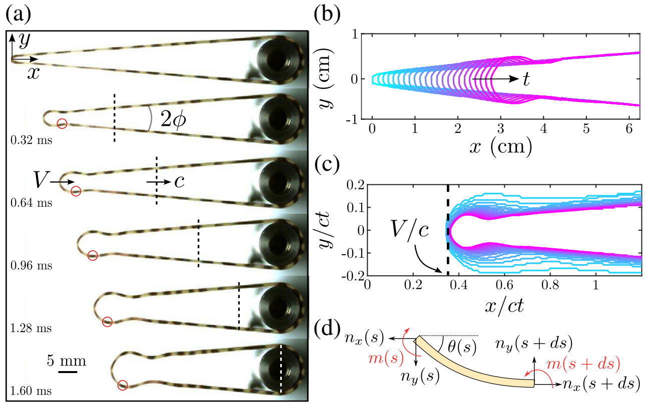

FIG. 2. (a) Marking material points on the elastic reveals a longitudinal shock traveling at speed $c = 43$ m/s, highlighted with a vertical dotted line. The material points behind the shock follow with an approximate velocity V and as a consequence move to different points of the curved region over time (red circles). Here $\phi = 4°$ and $\epsilon = 0.49$. (b) The shape of this retracting elastic can be extracted and plotted in spatial coordinates (x,y) at various times t. (c) Rescaling the spatial coordinates by the dynamic length scale ct illustrates that only the position of the end of the elastic is adequately captured in this self-similar framework, providing a value for the ratio V/c. (d) The dynamics of an elastic ribbon can be modeled in terms of the local angle θ, moment m, and projected internal forces n_x and n_y at each position s.

wave from which its speed c can be calculated. Here, $c = 43$ m/s is higher than the celerity $\sqrt{E/\rho} \approx 33$ m/s, where Young's modulus E and density ρ are directly computed for this elastic [see the Supplemental Material [13]]. This difference is likely due to the effect of strain rate [18], also observed in the retraction of flat elastic strips [15]. As the longitudinal wave travels toward the cylinder, material points trail behind it with a speed V directed along the x axis, which can be analyzed using the stretch ahead and behind the wave [19,20]. Indeed, the elastic is expected to be essentially relaxed after the wave passes, allowing us to estimate ℓ_0 from the arclength of the elastic when the longitudinal wave reaches the cylinder. The plucked string analysis also predicts that a transverse wave at the rear of the wedge would create a growing trapezoidal shape [19,20]. Yet, the shapes that we observe are curved and appear geometrically similar to one another as they evolve. Furthermore, the markings reveal that material points travel to different points around these curves as time progresses [red circles in Fig. 2(a)], suggesting a benefit in adopting an Eulerian, or spatial, description of the dynamics.

We set a fixed origin at the point of release, with the x axis oriented in the direction of motion. The spatial coordinates are extracted from the high-speed photographs using custom image processing and plotted at progressive times [Fig. 2(b)]. The lack of a geometric length scale associated with a wedge often leads to nongeometric properties combining to form a characteristic length scale that is a hallmark to self-similar dynamics. For example, self-similarities are manifested in retracting liquid wedges, which are driven by surface tension rather than elastic tension [21]. In our elastic wedge retraction, a natural time-varying length scale to consider is the distance ct the wave travels. Yet, when the shapes of the rubber band are plotted in these self-similar coordinates, they do not immediately collapse [Fig. 2(c)]. Nevertheless, the rear point of the elastic collapses to a particular value of x/ct, which is equivalent to the ratio V/c and can be used to estimate the speed of the rubber band.

To analyze the retraction speed, we model the region behind the longitudinal wave as an inextensible beam with width b and thickness h. This approximation for an initially loose elastic is supported by a more rigorous analysis that takes into account the amount of stretch [19]. The beam is parametrized by the unit arc length s as $\partial x/\partial s = \cos\theta(s,t)$ and $\partial y/\partial s = \sin\theta(s,t)$, where $\theta(s,t)$ denotes the angle between the tangent and the x axis. Assuming the absence of any external forces, such as gravity or air resistance, the balance of linear and angular momentum lead to the standard Kirchhoff equations, complemented by the constitutive laws for the tension within the beam and moment [22]

$$\frac{\partial n_x}{\partial s} = \rho b h \frac{\partial^2 x}{\partial t^2}, \qquad \frac{\partial n_y}{\partial s} = \rho b h \frac{\partial^2 y}{\partial t^2}, \tag{1a}$$

$$\frac{\partial m}{\partial s} + n_y \cos\theta - n_x \sin\theta = 0, \tag{1b}$$

$$n_x \cos\theta + n_y \sin\theta = E\epsilon b h, \qquad m = EI\frac{\partial\theta}{\partial s}. \tag{1c}$$

Here, n_x and n_y are the projected internal forces, m is the resultant bending moment, and $I = bh^3/12$ is the moment of inertia [Fig. 2(d)].

We first consider the case when the bending terms are negligible compared to the stretching terms ($\partial m/\partial s \ll n_y \cos\theta - n_x \sin\theta$). The expressions in Eq. (1) can be combined to obtain the wave equations $c^2\partial^2 x/\partial s^2 = \partial^2 x/\partial t^2$ and $c^2\partial^2 y/\partial s^2 = \partial^2 y/\partial t^2$. This form of the wave equation can also be obtained from a least action principle [23]. We seek self-similar solutions of the form $x/ct = X(\eta)$ and $y/ct = Y(\eta)$. Here, $\eta = s/ct$ is the self-similar variable and $X(\eta)$ and $Y(\eta)$ are the self-similar functions for the x and y components, respectively. These relations, in combination with the nonlinear wave equation, yield the following self-similar equations

$$(1-\eta^2)X''(\eta) = 0, \qquad (1-\eta^2)Y''(\eta) = 0, \tag{2}$$

where the prime denotes a differentiation with respect to η. Equation (2) yields the solutions, $\eta = 1$, $X'' = 0$, and $Y'' = 0$. Because we are interested in the region behind

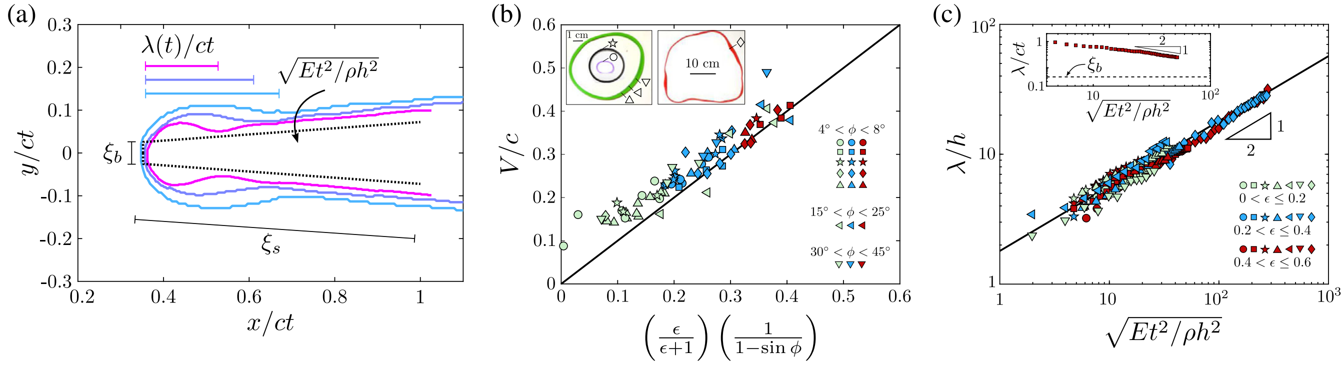

FIG. 3. (a) Experimental shapes from Fig. 2 rescaled on self-similar coordinates (x/ct, y/ct) reveal that the rescaled wavelength λ/ct decreases with time and thus likely depend on a combination of the thickness h, density ρ, and Young's modulus E. When the thickness h is negligible, the shape can be approximated as a trapezoid with dimensions ξ_b and ξ_s. (b) The retraction speed model (line) is consistent with measurements collected at various stretches and angles for different-sized rubber bands (symbols). (c) The measured wavelength λ for these elastics grows as $t^{1/2}$ and is independent of stain ϵ and angle ϕ. Inset: the rescaled wavelength for the elastic in Fig. 2 decreases with time as $t^{-1/2}$ and is larger than ξ_b during the entire retraction period.

the wave $\eta < 1$, we neglect the solution $\eta = 1$, as it reflects the position of the wave $s = ct$. The boundary conditions arise from the values of the tangent, which in self-similar form are $X'(0) = 0$, $X'(1) = \cos\phi$ for $X(\eta)$ and $Y'(0) = 1$, $Y'(1) = \sin\phi$ for $Y(\eta)$. These boundary conditions cannot be satisfied with a continuous curve, but can be satisfied with a trapezoidal shape.

To compute the position and size of the trapezoid, we combine geometric and kinematic arguments. When the wave reaches the cylinder, it has traveled a distance $ct = (\epsilon + 1)\ell_0 \cos\phi$. At that instant, half the trapezoid's self-similar length should be $\xi_s + \xi_b/2 = 1/[(\epsilon + 1)\cos\phi]$, where ξ_s and ξ_b are the trapezoid's side length and base length, respectively. Combining this relationship with the geometric condition $\tan\phi - \xi_s \sin\phi = \xi_b/2$, we calculate the lengths of the trapezoid as

$$\xi_s = \frac{1 - (\epsilon + 1)\sin\phi}{\cos\phi(\epsilon + 1)(1 - \sin\phi)}, \tag{3a}$$

$$\xi_b = 2\left(\frac{\epsilon}{\epsilon + 1}\right)\left(\frac{\tan\phi}{1 - \sin\phi}\right). \tag{3b}$$

The horizontal position of the base can be computed as $V/c = \xi_b/(2\tan\phi)$ so that

$$\frac{V}{c} = \left(\frac{\epsilon}{\epsilon + 1}\right)\left(\frac{1}{1 - \sin\phi}\right). \tag{4}$$

It is reassuring to note that in the extreme case $\phi \to 0$, the retraction speed in Eq. (4) reduces to $V/c = \epsilon/(\epsilon + 1)$, previously observed for cut, straight rubber strips [15].

Plotting the trapezoidal solution against the experimental shapes from Fig. 2, we find a consistency between theory and experiments [Fig. 3(a)]. The trapezoidal shape deviates from the experimental data only near the curved region, suggesting the importance of the neglected bending terms. By neglecting the bending terms in Eq. (1), we are assuming the thickness of the wedge to be negligible. Yet, as an intrinsic length scale in this system, the thickness is only negligible if it is small relative to the dominant length scale, here ct. This ratio of length scales can also be interpreted as a ratio of bending and stretching effects and gives rise to the dimensionless parameter $\sqrt{Et^2/\rho h^2}$. Therefore, assuming the thickness to be negligible $h \to 0$ is equivalent to considering the shape at an arbitrarily long time $t \to \infty$. As $\sqrt{Et^2/\rho h^2}$ increases, the rescaled wavelength λ/ct becomes progressively smaller, eventually converging to the trapezoidal solution [Fig. 3(a)].

Conversely, as $\sqrt{Et^2/\rho h^2}$ decreases, the importance of thickness h becomes progressively larger, motivating us to consider the case when the stretching terms are negligible compared to the bending terms. Following the analysis of Audoly and Neukirch under the assumption of small displacements [10], the Kirchhoff equations (1) can be simplified to

$$EI\frac{\partial^4\theta}{\partial s^4} + \rho bh\frac{\partial^2\theta}{\partial t^2} = 0, \tag{5}$$

which indicates the balance of solely bending and inertia. A natural length scale for this equation is $[(EIt^2)/(\rho bh)]^{1/4}$, and we therefore seek self-similar solutions using the variable $\tilde{\eta} = s/(Eh^2t^2/12\rho)^{1/4}$. It is convenient to solve for the complementary angle $u(\tilde{\eta}) = \pi/2 - \theta(s, t)$, which when substituted into Eq. (5) reduces to

$$4u''''(\tilde{\eta}) + \tilde{\eta}^2 u''(\tilde{\eta}) + 3\tilde{\eta}u'(\tilde{\eta}) = 0. \tag{6}$$

This differential equation is identical to that obtained by Audoly and Neukirch when modeling fragmentation due to focused bending [10], with the key difference being that our equation is in terms of the angle rather than the curvature.

Solving Eq. (6) requires four boundary conditions. Symmetry provides boundary conditions $u(0) = 0$ and $u''(0) = 0$, whereas the far-field angle prescribes a third $u(\infty) \to (\pi/2 - \phi)$. The last boundary condition, $u'''(0) = 0$, is a consequence of the dynamic beam equation: $EI\partial^4 y/\partial s^4 + \rho bh\partial^2 y/\partial t^2 = 0$. Specifically, because $y(0, t) = 0$, the origin does not accelerate leading to $\partial^4 y/\partial s^4(0, t) = 0$, or equivalently $u'''(0) = 0$. These boundary conditions lead to the self-similar solution, $u(\tilde{\eta}) = (\pi - 2\phi)\mathcal{C}(\tilde{\eta}/\sqrt{2\pi})$, where $\mathcal{C}(\tilde{\eta}) = \int_0^{\tilde{\eta}} \cos[(\pi/2)\eta^2]d\eta$, is the Fresnel cosine integral. This solution has a finite curvature at the origin, as contrasted with Ref. [10]. The equation for u suggests that the wavelength λ should occur when $\tilde{\eta} = 2\sqrt{\pi}$. Under the assumption of small displacement, $s \approx x - Vt$, the wavelength can be defined as $\lambda = 2\sqrt{\pi}(Eh^2t^2/12\rho)^{1/4}$. Note that λ is independent of both strain ϵ and far-field angle ϕ.

To test these predictions for V/c and λ, we carry out systematic experiments with a variety of rubber bands of different sizes. These rubber bands span circumferences between 5.4 and 91.4 cm, while having similar densities, Young's moduli, and thicknesses [see the Supplemental Material [13]]. Experimental values of the velocity ratio V/c are plotted in Fig. 3(b) for different-sized rubber bands (symbols, see inset) by varying the strain (color) and wedge angle (orientation) and reasonably agree with the theoretical relationship (solid line) of Eq. (4). Similarly, by plotting the normalized wavelength λ/h against the dimensionless group $\sqrt{Et^2/\rho h^2}$ on logarithmic scales, it becomes apparent that the wavelength grows as $\lambda \sim \sqrt{t}$ [Fig. 3(c)]. This behavior is found in many problems associated with flexural waves in rods and beams [10,24,25], indicating that the growing curved region is in fact a bending wave. Indeed, the best-fit prefactor of 1.8 shown in Fig. 3(c) is close to $2\sqrt{\pi}/(12)^{1/4} \approx 1.9$ from our analysis. Furthermore, the data in Fig. 3(c) indicated that the wavelength is independent of the wedge angle and initial strain, also predicted in our analysis. Therefore, even though the appropriateness of the small-angle approximation is questionable, it provides a reasonable estimate for the wavelength and its dependencies.

To predict when bending effects will influence the shape of the retracting elastic wedge, it is instructive to return to Fig. 3(a). Note that the influence of the wavelength λ on the overall shape of the retracting rubber band diminishes with time as $\lambda/ct \to 0$. This effect is quantified in the inset of Fig. 3(c), which illustrates two important points: the rate of this decrease scales as $t^{-1/2}$ and the values throughout the entire retraction period are greater than ξ_b. Had the retraction continued, it is expected that the values of λ/ct would eventually be smaller than ξ_b, at which point the trapezoidal shape would dominate. Indeed, the value of

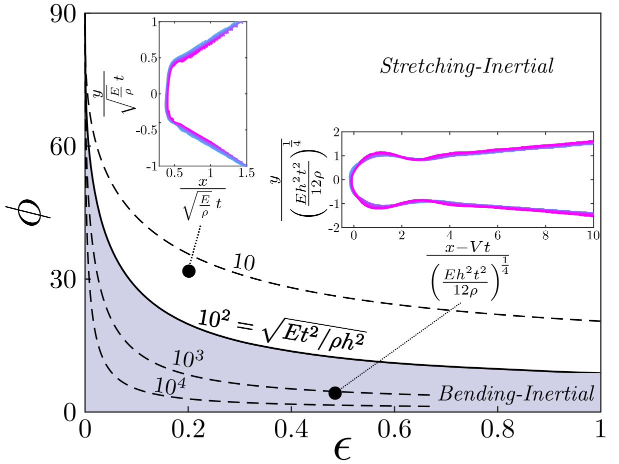

FIG. 4. Theoretical phase diagram illustrating the conditions predicted for a bending-dominated retraction regime (shaded region). The boundary depends on the strain ϵ, wedge half-angle ϕ, and the dimensionless number $\sqrt{Et^2/\rho h^2}$. Top-left inset: in the stretching-dominated regime, the shapes collapse using the self-similar scalings $x/\sqrt{(E/\rho)}t$ and $y/\sqrt{(E/\rho)}t$. Bottom-right inset: in the bending-dominated regime, the shapes collapse using the self-similar scalings $[(x - Vt)/(Eh^2t^2/12\rho)^{1/4}]$ and $[y/(Eh^2t^2/12\rho)^{1/4}]$.

ξ_b can be interpreted as the velocity that a transverse elastic wave travels along the y axis. Thus, we can estimate whether the retraction will be dominated by stretching or bending by computing the ratio of the trapezoid base to the rescaled wavelength. This analysis predicts that the shape will be bending dominated provided that the elastic is stretched less than

$$\epsilon < \frac{1 - \sin\phi}{(\frac{12}{\pi^2})^{1/4}(\frac{Et^2}{\rho h^2})^{1/4}\tan\phi + \sin\phi - 1}. \quad (7)$$

Equation (7) can be used to develop a phase diagram to predict when a bending-dominated regime will occur based on the initial strain and the wedge half-angle (Fig. 4). In particular, the boundary separating the two regimes depends on the time-dependent dimensionless parameter $\sqrt{Et^2/\rho h^2}$. At early times, the bending-dominated regime is prominent for moderate wedge half-angles. As time increases, the boundary moves in favor of the stretching-dominated regime, reducing the extent of the bending regime to small strains and wedge half-angles. Considering the entire retraction period, we choose to set a characteristic boundary at $\sqrt{Et^2/\rho h^2} = 100$ using an order-of-magnitude approximation for the parameters of a stereotypical shot rubber band [26], such as the one shown in Fig. 1. An elastic stretched at moderate wedge angles will initially retract in the bending regime. However, its retraction period is sufficiently long to transition to the stretching regime [see the Supplemental Material [13]]. By contrast, an elastic stretched at small angles does not retract for a sufficiently long time and remains in the bending-dominated regime throughout its retraction. In this regime, the shapes can be collapsed into self-similar coordinates using the scaling associated with bending $(Eh^2t^2/12\rho)^{1/4}$, where Vt is subtracted from the x coordinate. Indeed, all of the curves in Fig. 2 collapse onto a single curve with this scaling (top right inset in Fig. 4). Conversely, the retracting shapes within the stretching regime can be collapsed to a self-similar trapezoid using the scaling $\sqrt{E/\rho}t$ (see top left inset in Fig. 4).

Taken together, our analysis and experimental data extend previous studies of elastic retraction to consider a stretched elastic wedge with finite thickness. We find that for the small wedge angles typical when shooting rubber bands, the retraction can be described by a distinct self-similar curve with a dynamic length scale arising from a balance of inertia and bending. Within this bending regime, the strain and wedge angle do not significantly influence the shape but do affect the retracting velocity. We find that this velocity can be adequately estimated by the same kinematic and geometric relationships in both regimes. The boundary between the two regimes depends on three dimensionless groups, the wedge half-angle ϕ, the strain ϵ, and the parameter $\sqrt{Et^2/\rho h^2}$. These dynamics can provide further insight into retracting systems in which there is a high energetic cost to curvature and could be extended for a viscous environment [15] that would be expected for small-scale applications such as molecular drug delivery.

From a curiosity-driven perspective, the results highlight how—when a rubber band is fired off a thumb—the thumb can avoid being hit by the elastic. Tension from the stretched elastic is counteracted by a torque exerted by the thumb; the tension suddenly vanishes when the longitudinal wave reaches the thumb, causing the thumb to inadvertently deflect. Because the longitudinal wave is faster than the elastic, there can be enough time for the thumb to adequately deflect, with this time depending on the ratio V/c in the bending-dominated regime [27].

We thank P. Barbone, D. P. Holmes, C. F. Brasz, and M. Pezzulla for helpful discussions.

*Corresponding author.
jbird@bu.edu

[1] G. F. Wheeler and W. P. Crummett, Am. J. Phys. **55**, 33 (1987).
[2] N. H. Fletcher and T. D. Rossing, *The Physics of Musical Instruments* (Springer Science & Business Media, Berlin, 2012).
[3] C. N. Hickman, J. Appl. Phys. **8**, 404 (1937).
[4] S. Ranallo, C. Prévost-Tremblay, A. Idili, A. Vallée-Bélisle, and F. Ricci, Nat. Commun. **8**, 15150 (2017).
[5] R. B. Stambaugh, Rubber Chem. Technol. **17**, 617 (1944).
[6] B. A. Stambaugh, S. L. Dart, and E. Guth, Phys. Rev. **66**, 30 (1944).
[7] B. A. Stambaugh, S. L. Dart, and E. Guth, Phys. Rev. **66**, 32 (1944).
[8] H. M. James and E. Guth, Phys. Rev. **66**, 33 (1944).
[9] A. N. Gent and P. Marteny, J. Appl. Phys. **53**, 6069 (1982).
[10] B. Audoly and S. Neukirch, Phys. Rev. Lett. **95**, 095505 (2005).
[11] B. Audoly and Y. Pomeau, *Elasticity and Geometry: From Hair Curls to the Non-Linear Response of Shells* (Oxford University Press, Oxford, 2010).
[12] A. C. Callan-Jones, P.-T. Brun, and B. Audoly, Phys. Rev. Lett. **108**, 174302 (2012).
[13] See Supplemental Material at http://link.aps.org/supplemental/10.1103/PhysRevLett.122.014102 for material and geometric properties of the rubber bands used in the experiments, as well as additional details for the regime transition and thumb movement. Videos of shooting rubber bands are also included.
[14] J. R. Gladden, N. Z. Handzy, A. Belmonte, and E. Villermaux, Phys. Rev. Lett. **94**, 035503 (2005).
[15] R. Vermorel, N. Vandenberghe, and E. Villermaux, Proc. R. Soc. A **463**, 641 (2007).
[16] R. C. Cross and M. S. Wheatland, Am. J. Phys. **80**, 1051 (2012).
[17] P. Mason, Proc. R. Soc. A **272**, 315 (1963).
[18] H. Kolsky, Proc. Phys. Soc. London Sect. B **62**, 676 (1949).
[19] J. L. Wegner, J. B. Haddow, and R. J. Tait, J. Appl. Mech. **56**, 459 (1989).
[20] J. L. Wegner and J. B. Haddow, J. Appl. Mech. **57**, 667 (1990).
[21] J. B. Keller and M. J. Miksis, SIAM J. Appl. Math. **43**, 268 (1983).
[22] B. D. Coleman and E. H. Dill, J. Acoust. Soc. Am. **91**, 2663 (1992).
[23] J. A. Hanna, Int. J. Solids Struct. **62**, 239 (2015).
[24] Z. J. Bilek and S. J. Burns, J. Mech. Phys. Solids **22**, 85 (1974).
[25] K. F. Graff, *Wave Motion in Elastic Solids* (Dover Publications, New York, 2012).
[26] For the rubber band in Fig. 1, the retraction period lasts approximately $t = 3$ ms. Applying a rough approximation using orders of magnitude ($t^2 \approx 10 \times 10^{-6}\,\mathrm{s}^2$, $E \approx 10^6\,\mathrm{Pa}$, $\rho \approx 10^3\,\mathrm{kg/m^3}$, and $h^2 \approx 10^{-6}\,\mathrm{m}^2$) leads to $\sqrt{Et^2/\rho h^2} = 100$.
[27] A simple scaling argument can be derived to relate the time required to deflect the thumb within the time available to deflect it. The elastic will pass over the thumb when $\epsilon(r^2 d^2 \alpha/\ell_0^2 bh)(\rho/\rho_t) \lesssim 1$, where ℓ_0 is the elastic length, α is the deflection angle, and ρ_t, r, and d are the density, radius, and length of the thumb [see the Supplemental Material [13]].